

## Article

# Electromechanical Property Calculation of Carbon Nanotubes Using Linear Augmented Cylindrical Wave Method

Pavel D'yachkov

Kurnakov Institute of General and Inorganic Chemistry of the Russian Academy of Sciences, Leninskii pr. 31, 119991 Moscow, Russian Federation: p\_dyachkov@rambler.ru

Received: May 23, 2022; Accepted: Jun 23, 2022; Published: Jun 30, 2022

**Abstract:** Deformations of single-walled carbon nanotubes (SWNTs) change their band structure in the nanoelectromechanical systems. In this study, we investigated the response of the electronic structure of chiral and nonchiral SWNTs (8,7), (9,6), (10,5), (7,7), (11,0), (12,0), and (13,0) to twisting and axial tension modes by using the symmetrized linear augmented cylindrical wave technique. We showed that perturbations of the band structures depend on a “family” index  $p = (n_1 - n_2) \bmod 3$  (where  $p = -1, 0$  or  $1$ ). Twisting the semiconducting (8,7) tubule with  $p = 1$  in the direction of the screw axis is accompanied by the large broadening of minimum gap  $E_{11}$  and narrowing of the second gap  $E_{22}$ , while these gaps drastically change in the tubule (10,5) with  $p = -1$ . In these tubules, changing the direction of twisting leads to the reversal in direction of the gap shifts. Regardless of the twisting direction, in metallic (7,7) and quasi-metallic (9,6) SWNTs with  $p = 0$ , the  $E_{11}$  gap rapidly increases from 0.0 and 0.035 eV to about 1 eV. When twisting the zigzag tubules (13,0)  $p = 1$  and (11,0)  $p = -1$ , the gaps  $E_{11}$  equal to about 0.8 eV increase and decrease by several hundredths of eV. On the contrary, the compression and extension of these tubules cause a sharp change in their band structure with approximately a twofold change in the gaps  $E_{11}$  and  $E_{22}$  and inversion in the sequence of the boundary bands. The similar deformation of the armchair nanotube (7,7) has practically no effect on its electronic levels. In the case of zigzag (12,0)  $p = 0$  SWNT, all deformation modes transform the quasi-metallic tubule into the semiconductor.

**Keywords:** Carbon nanotubes, Nanoelectromechanics, Modelling, Electron cylindrical waves technique

## 1. Introduction

In recent years, a large number of studies on electromechanical characteristics of carbon nanotubes have been carried out. The single-walled nanotubes (SWNTs) are cylindrical molecules that can be viewed as the results of rolling up the graphene ribbons into seamless tubules [1]. Their geometry is completely specified by the two positive integers  $(n_1, n_2)$ , where  $n_1 \geq n_2 \geq 0$ , or by the diameter  $d$  and chirality angle  $\theta$ . The  $(n, n)$  and  $(n, 0)$  SWNTs have an inversion symmetry and are nonchiral, therefore. Other tubules are characterized by the right-handed or left-handed helical axis and are chiral. The chirality indices determine the band structures of SWNTs [2–8]. Depending on the diameter and chirality, the tubules have metallic, semiconducting, or quasi-metallic properties with great potential applications in nanoelectronics. They have low density and ultrasmall cross-section and are defect-free [8]. Relative to their diameter, the SWNTs are the stiffest and strongest springs [9,10], but if nanotubes are subjected to deformation, their electronic properties change. By stretching, contracting, twisting, and bending the SWNTs, the electronic bandgaps are opened in certain metallic nanotubes and modified in the semiconducting tubules. An atomic force microscope (AFM) experiments show that the linear electromechanical responses are observed for the axial [11–13], radial [14], flexural [15], and torsional strains [16] in SWNTs as the tubules act as the transistors to sense their motion. All of this points to the remarkable possibilities of using SWNTs as the basic ingredients of nanoelectromechanical systems (NEMS) which are devices combining the electrical and mechanical properties of carbon nanotubes [17,18]. As an example, a variety of electromechanical resonators on nanotubes are used in atomic-scale mass sensors, ultrasensitive force detectors, and nanotube radio devices [18–22].

Since such devices have both electronic and mechanical degrees of freedom, it is of great importance to know how the electronic band structures change upon the SWNTs deformations. First, the effects of small uniaxial, bending, and torsional strains on the band-gap perturbation of the achiral and chiral SWNTs were analyzed neglecting the nanotubes curvature and applying the simple  $\pi$ -electron Hückel approach combined with graphene zone-folding technique to describe the carbon bond network of the SWNTs via a single nearest-neighbor hopping parameter [23–26]. This simple Hamiltonian lacks the accuracy that sophisticated models provide. Several studies based on the tight-binding (TB) method, four-orbital extended Hückel method, and two-center parameterization of carbon have been carried out to simulate SWNTs under tension, bending, and twisting [23,24,27,28]. Using the

same semi-empirical Hamiltonian, the variations of the local density of states and conductance due to the bending and twisting of the cluster containing 948 C atoms arranged in an armchair (6,6) structure were studied [29], and the energy gaps formation in a wider range of armchair SWNTs having the regions of local twists (twistons) were estimated [30]. The cluster calculations of the effects of nanotubes geometry change due to indentation with a sharp AFM tip were simulated using the density functional TB method too [31,32].

Going beyond the cluster models and semiempirical tight-binding approaches, several first-principles-based calculations on this subject have been reported to date [33–39]. Most of the *ab initio* calculations focus on the standard examples of the nonchiral armchair and zigzag SWNTs [33–44] because chiral tubules have typically large numbers of atoms  $N_{tr}$  per translational unit cell. For example, the  $N_{tr} = 40$  for the achiral (10,10) SWNT, but  $N_{tr} = 1084$  for the chiral (10,9) tubule that has a smaller diameter. The first-principle calculations of the chiral tubules and the effects of torsional deformations require special approaches with helical symmetry operations because twisting the tube at even a small angle increases the size of the tube's translation cell infinitely, and the usual translation-invariant formulation is computationally prohibitive for long-range deformations with helical symmetry [6,7,36–39]. Moreover, the torsions are the intrinsically chiral modes, they continuously vary the chirality angle and particularly turn the achiral SWNTs into chiral objects [45]. Nevertheless, using the symmetrized TB approach, several *ab initio* calculations of the chiral nanotubes and the effects of torsional deformations on the electronic properties of nanotubes have already been presented. In Ref. [36], the simplest case of the formation of optical gaps between the highest occupied and lowest unoccupied molecular orbitals (HOMO and LUMO) in the metallic nonchiral armchair ( $n, n$ ) tubes with  $n$  from 6 to 25 due to their twisting was considered. For several chiral tubes, the perturbations of the HOMO-LUMO gap widths were calculated as a function of the torsional deformation [38,39]. However, under the mechanical deformations of the SWNTs, not only the minimum optical gaps are to be formed or changed, but the entire band structure of tubules is to be distorted.

The purpose of this study is to fill this gap by performing the more complete first-principle calculations of the response of the band structures of chiral and nonchiral SWNTs to the twisting modes and studying the effects of the axial tension. Here, we apply a linearized augmented cylindrical wave (LACW) method in detail which fully utilizes the rotational and helical symmetries and allows dealing with helical configurations of SWNTs without translational periodicity [46–50]. In contrast to the TB method with a purely localized set of basis functions, there are both the localized and delocalized components in LACW basis functions, which gives advantages for the quantitative description of the energy levels of the conduction band. The main argument for using cylindrical waves exists for the cylindrical geometry of the nanotubes in an explicit form that offers obvious advantages. Because of the potential applications of SWNTs as components of NEMS, the extensive quantitative studies on their electron structure change due to twisting, stretching, and contraction are important.

## 2. Materials and Methods

The structure of any SWNT can be generated by mapping two nearest-neighbor C atoms onto a cylindrical surface and then applying the rotational  $C_n$  and helical  $S(h_z, \omega)$  symmetry operations to determine the remainder of the tubule [8]. In SWNTs, the  $C_n$  rotational axis coincides with the cylindrical axis of the system,  $n$  being the largest common divisor of the  $n_1$  and  $n_2$ . The screw operations  $S(h_z, \omega)$  are the repeated rotations at the angles  $\omega$  about the tubule axis with translations  $h_z$ , which depend on the  $n_1$  and  $n_2$  values and determine the helical geometry of SWNTs. Later in the text, we assume that  $S(h_z, \omega)$  is the right-handed screw operation along the positive axis of the tubule with a positive helical angle  $\omega$  around this axis.

In the LACW method, the helical and rotational symmetry properties of the tubules are taken into account. The true unit cell of any SWNT is reduced to only two carbon atoms, and calculations of any nonchiral or chiral tubule with twisting deformation are possible as it is independent of the enormous numbers of atoms per translational cell without introducing unwanted end effects and cluster models. The LACW method is an extension of the case of tubular compounds of the linear augmented plane-wave (LAPW) method that is well-known in the theory of bulk solids as one of the most accurate techniques for calculating the band structures [51–54]. Similar to the LAPW technique, the LACW approach applies the muffin-tin (MT) and local density approximations for the electronic potential. The helical and rotational symmetry properties of tubules are taken into account when writing the basis functions and Hamiltonian. The rigorous justification of method and explicit equations for the basis functions and secular equations are given in this study and recent monograph [46–49]. The eigenfunctions  $\Psi_\lambda(\mathbf{r}|\mathbf{k}, L)$  and energies  $E_\lambda(\mathbf{k}, L)$  of the electronic Hamiltonian depend on the wave vector  $\mathbf{k}$  ( $0 \leq k \leq \pi/h_z$ ) and on the rotational quantum number  $L = 0, 1, \dots, n - 1$ , labeling the standing electronic waves in the circumferential direction. The geometry parameters  $h_z$  and  $\omega$  of SWNT are used as input data. LACW calculations are performed for any tubule and any external twisting angle  $\Delta\omega$  or axial tension  $\Delta h_z$  with the same number of computational efforts. The band structures of deformed nanotubes can be best demonstrated in the most complete form applying a doubly repeated zone scheme.

### 3. Results and Discussion

Let us consider the effects of the twisting and axial tension modes on the band structures of the SWNTs (8,7), (9,6), (10,5), (7,7), (11,0), (12,0), and (13,0) with virtually equal diameters between 10 and 11 Å, but different chiralities. We restrict the twisting and tension amplitudes  $\Delta\omega$  from  $-2^\circ$  up to  $2^\circ/\text{\AA}$  and  $\Delta h_z$  between  $-5$  and  $5\%$ , since the ideal cylindrical geometry of nanotubes can still be preserved within these limits. However, further twisting or tension leads to the buckling and development of rippling deformation with ridges and furrows on their surface, and conductance irreversibly drops beyond the critical deformations [10,16,36]. The band properties of the ideal SWNTs not subjected to deformations are characterized by the “family index”  $p = (n_1 - n_2) \bmod 3$ . The SWNTs with  $p = 0$  are known to be metallic if  $n_1 = n_2$  or quasi-metallic if  $n_1 \neq n_2$ , and tubes with  $p = 1$  and  $p = -1$  are the semiconductors. Therefore, there are both chiral and nonchiral, metallic, quasi-metallic, and semiconducting nanotubes with all  $p$  indices in this representative series.

#### 3.1. Chiral SWNTs

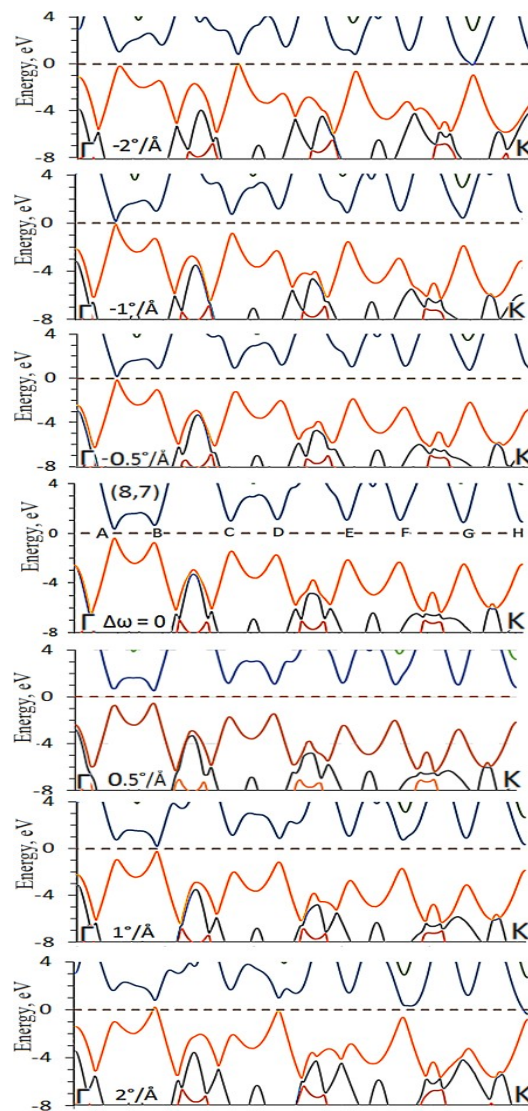


**Fig. 1.** Band structure changes under twisting the (8,7) SWNT. Zero-point energy is at the Fermi level.  $\Gamma$  and K points correspond to wave vector  $k = 0$  and  $k = \pi/h_z$ .

Figure 1 shows the first example of calculations, namely, the band structure changes under twisting the chiral (8,7) tubule having as many atoms as 676 per translational unit cell. For the undistorted structure,  $\Delta\omega = 0$ , the Fermi level separates the valence and conduction band dispersion curves, and this nanotube is the semiconductor with the minimum direct energy gap  $E_g = 0.76$  eV

corresponding to the transition at the A point of the Brillouin zone with  $k = 0.9 \pi/h_z$ . The next minimum gap  $E_g = 1.42$  eV is located at the B point with  $k = 1.8 \pi/h_z$ . The energies of other direct gaps located at the C, ..., H points are equal to about 2.5–3.5 eV.

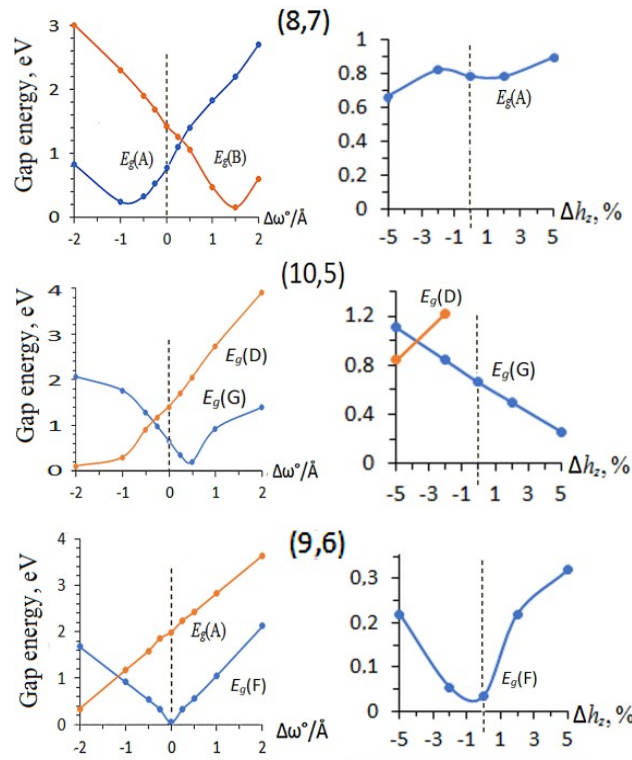


Fig. 2. Variations of minimum direct gaps of chiral nanotubes due to torsional  $\Delta\omega$  and axial  $\Delta h_z$  deformations.

The variations of electron structure depend on the twisting direction. Figure 2 shows the two minimum band gap energies as the functions of twist angle  $\Delta\omega$ . Twisting the tube in the helical axis direction at the angles  $\Delta\omega = 0.5$  and  $1^\circ/\text{\AA}$  results in the increase of  $E_g(A)$  gap up to the 1.45 and 1.8 eV. The LACW calculations confirm the positive sign of the derivative of the minimum gap  $dE_g(A)/d\Delta\omega$  at the  $\Delta\omega = 0$  obtained originally by using the explicit formulas of the  $\pi$ -electronic Hückel approach for the tubes of the series  $p = 1$  [23,24], but the  $E_g(B)$  gap gets smaller from 1.42 eV down to 1.1 and 0.46 eV due to these deformations. The derivative  $dE_g(B)/d\Delta\omega$  is negative at the  $\Delta\omega = 0$ . Therefore, for the  $\Delta\omega > 0$ , the width of the forbidden gap initially grows from 0.76 eV up to 1.4 eV, and then, at about  $\Delta\omega = 0.5^\circ/\text{\AA}$ , it jumps from points A to B and finally decreases down to 0.14 eV at  $\Delta\omega = 1^\circ/\text{\AA}$ . The twisting by the  $\Delta\omega = -0.5$  and  $-1^\circ/\text{\AA}$  that is, twisting of the tube against the chirality axis, induces the reverse shifts of the gaps  $E_g(A)$  and  $E_g(B)$ . At the A point, the gap decreases from 0.76 eV to about 0.33 and 0.24 eV for  $\Delta\omega = -0.5$  and  $-1^\circ/\text{\AA}$ , respectively. At the B point, the  $E_g(B)$  gap shift is positive. The  $E_g(B)$  gap grows from about 1.4 at the  $\Delta\omega = 0$  to 1.9 and 2.3 eV at  $\Delta\omega = -0.5$  and  $-1^\circ/\text{\AA}$ . An increase in the twisting angle in the region  $-1^\circ/\text{\AA} \leq \Delta\omega \leq 1^\circ/\text{\AA}$  results in approximately linear growth of the energies of the direct transitions at points A, C, and E, and by a similar decrease of the transition energies at points B, D, G, F, and H. The further twisting of the tubule with angles  $\Delta\omega = \pm 2^\circ/\text{\AA}$  leads to the overlap of the valence and conduction bands and metallization of the semiconducting SWNT (8,7). At the  $\Delta\omega = 2^\circ/\text{\AA}$ , the conduction band minimum is located at the H point below the Fermi level by 0.18 eV and the valence band maximum, at the B point of the Brillouin zone above the Fermi level by approximately the same value. With negative twisting of  $-2^\circ/\text{\AA}$ , the  $E_v(C)$  and  $E_c(G)$  levels overlap by  $\sim 0.05$  eV. Figure 2 shows that the stronger twisting deformation of the tube is accompanied by its further metallization due to the increase of intersection points of the valence and conduction band states.

As expected for so-called “near-armchair” SWNTs [39] and in sharp contrast to twisting, the stretching and compression weakly perturb the electronic structure of the (8,7) SWNT. When its length is varied within  $\pm 5\%$ , the level shifts in the valence and conduction bands are about  $\pm 0.1$  eV only. In particular, the minimum gap  $E_g(A)$  lies in the range 0.66–0.9 eV (Fig. 2).

Figure 3 shows how twisting induces the variations of electronic properties of the (10,5)  $p = -1$  chiral nanotube characterized by the fifth-order rotational axes. The band structure is presented applying the repeated zone scheme, according to which the bands for rotational quantum number  $n - L$  are the extensions of the bands for  $L$  [46]. At the  $\Delta\omega = 0$ , the minimum gap with energy  $E_g = 0.66$  eV is located at the G point with  $L = 2$ , and the second gap with  $E_g = 1.6$  eV at the D point with  $L = 4$ . At the twisting angle

range between 0 and  $0.5^\circ/\text{\AA}$ , the  $E_g(G)$  value falls to 0.24 eV, and it grows up to 0.92 eV with a further increase in  $\Delta\omega$  to  $1^\circ/\text{\AA}$ . At negative values of the  $\Delta\omega$ , the main  $E_g(G)$  gap rapidly increases up to 2 eV, but the  $E_g(D)$  gap drops to 0.3 eV. The  $E_g(G)$  and  $E_g(D)$  gap dependences of  $\Delta\omega$  intersect at the twisting angle  $\Delta\omega \approx -0.25^\circ/\text{\AA}$ . With further deformation, the  $E_g(D)$  gaps are significantly smaller than the  $E_g(G)$  gaps. Similar to the case of the (8,7) tubule, there is a crossing of the valence and conduction bands at  $\Delta\omega = \pm 2^\circ/\text{\AA}$ , and the nanotube becomes metallic. This tube belongs to the series  $p = -1$ , and the derivative of the main gap  $dE_g(G)/d\Delta\omega$  is negative at the  $\Delta\omega = 0$  [23,24], but the sign of the  $dE_g(D)/d\Delta\omega$  is positive. Similar to the (8,7) tubule, a picture of the changes in the band structure under the action of a nanotube (10,5) twisting becomes complicated as compared to the predictions of the  $\pi$ -electron approximation. The stretching and compression of the tubule (10,5) within 5% leads to about a twofold decrease and increase in the gap  $E_g(G)$  to 0.26 and 1.11 eV. Figure 2 shows that the dependence of  $E_g(G)$  on the  $\Delta h_z$  is linear, simpler than the dependence of  $E_g(G)$  on the  $\Delta\omega$ , which has a form of the curve with a sharp minimum of about  $\Delta\omega = 0.5^\circ/\text{\AA}$ .

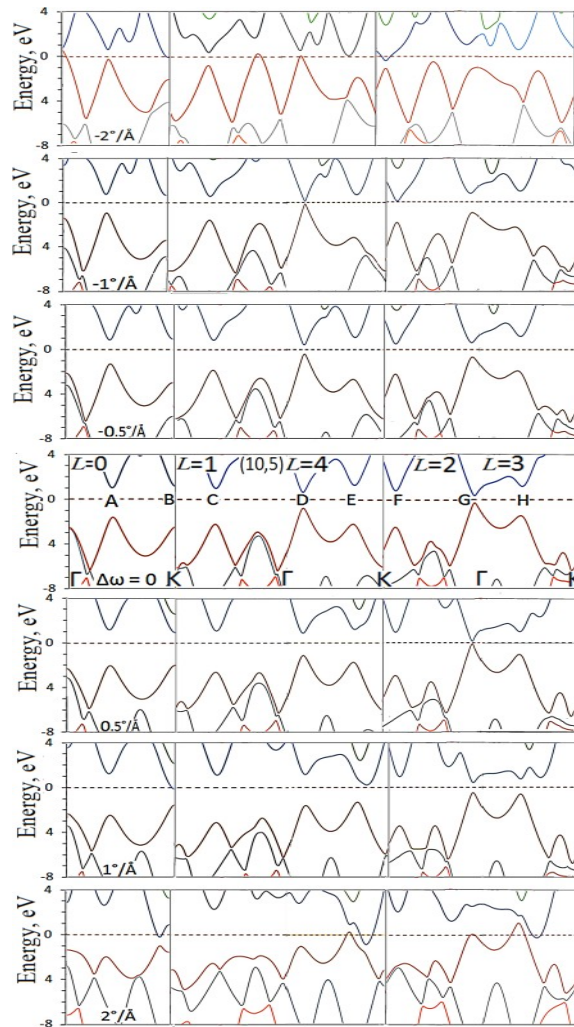


Fig. 3. Band structure changes under twisting the (10,5) SWNT.

The (9,6) SWNT with  $p = 0$  has the rotational third order axis  $C_3$ , and the eigenstates depend on the wave vector  $k$  and the rotational quantum number  $L = 0, 1$ , and  $2$ . Figure 4 shows the evolution of the band structure of this SWNT under twisting. According to the simple Hückel method, the untwisted tubule must have a metallic type band structure with zero forbidden gap, but the LACW approach predicts the formation of the mini-gap  $E_g = 0.035$  eV at F the point on the border between the states with  $L = 1$  and  $L = 2$  and  $k \approx 0$  caused by tubule's cylindrical surface curvature. The energies of other direct gaps are not less than 2 eV. Being independent of the direction of weak twisting angle  $\Delta\omega = \pm 0.25^\circ/\text{\AA}$ , the energy of transition  $E_g(F)$  increases to 0.34 eV. Further twisting the nanotube in the positive and negative directions leads to a monotonic growth of the  $E_g(F)$  gap up to the 1.0, 0.9, 2.1, and 1.8 eV at the  $\Delta\omega = 1, -1, 2$ , and  $-2^\circ/\text{\AA}$ . The  $\Delta\omega$  dependence of  $E_g(F)$  is almost symmetric relative to the  $\Delta\omega$  sign change [23,24]. As to the second minimum gap  $E_g$  located at point A, it is sensitive to twisting. The change of the  $\Delta\omega$  angle from  $-2$  to  $2^\circ/\text{\AA}$

results in the decrease of the gap from  $E_g = 3.6$  to  $E_g = 0.6$  eV. For  $\Delta\omega \leq -1^\circ/\text{\AA}$ , the  $E_g(\text{A})$  gap is smaller than the main gap  $E_g(\text{F})$ . In the case of the large positive  $\Delta\omega$  angles, the growth of the gap at the F point is accompanied by a drastic decrease in the gaps at  $E_g(\text{G})$  ( $L = 2$ ) and  $E_g(\text{D})$  ( $L = 1$ ) resulting finally in the closure of these gaps at the twisting angle equal to  $2^\circ/\text{\AA}$ . The large negative twisting angle with  $\Delta\omega = -2^\circ/\text{\AA}$  leads to the formation of the conducting states at the A and C points with  $L = 0$  because the Fermi level crosses the corresponding curves. For both the right and left twisting, the minimum band gap initially increases, then jumps to some new point of the Brillouin zone, decreases, and vanishes.

The stretching and compression of the (9,6) tubule along the z-axis are also accompanied by an increase in the energy of the minimum gap  $E_g(\text{A})$ , but it is limited to 0.3 eV only in the studied range of deformations. That is, it is an order of magnitude smaller than the effect of twisting (Fig. 2). Under uniaxial deformations, the displacements of other electronic levels and gaps are insignificant.

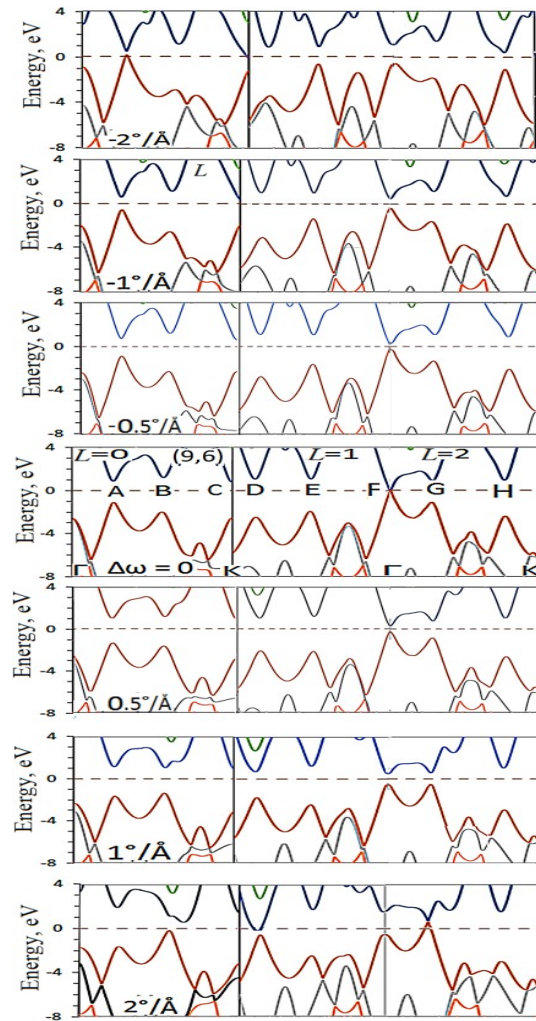


Fig. 4. Band structure changes under twisting the (9, 6) SWNT.

### 3.2. Armchair SWNTs

For the simpler cases of the nonchiral SWNTs starting from the (7,7) armchair tubule, when the achiral nanotube is twisted, the band structure variations do not depend on the twisting direction due to the symmetry. The tubules twisted for the  $\Delta\omega$  and  $-\Delta\omega$  are the mirror images, and their electronic structures are to be identical. Thus, the positive  $\Delta\omega$  strains are dealt with only. Figure 5 shows that in the stress-free case the (7,7) nanotube has the metallic type band structure because of a crossing of  $\pi$ -bands at the A point with  $L = 0$  and  $k = 2\pi/3h_z$ . The energies of all other gaps are equal to between 2.1 and 3.5 eV.

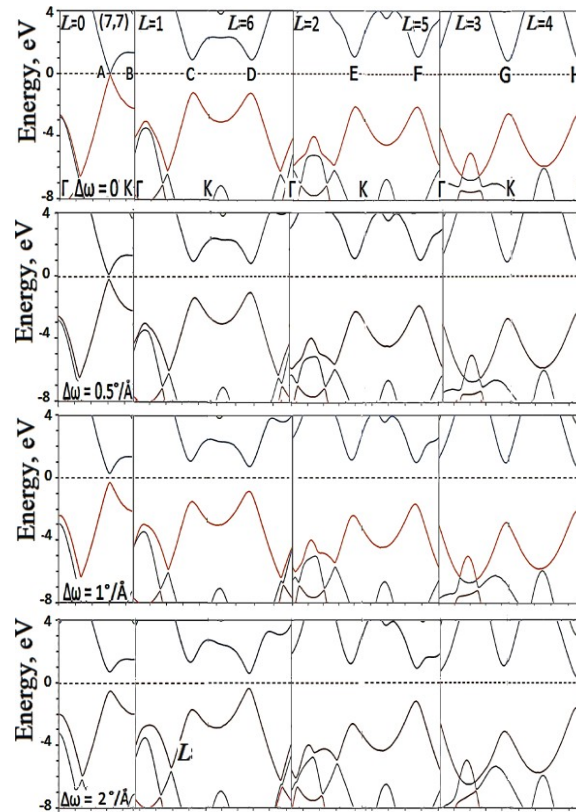
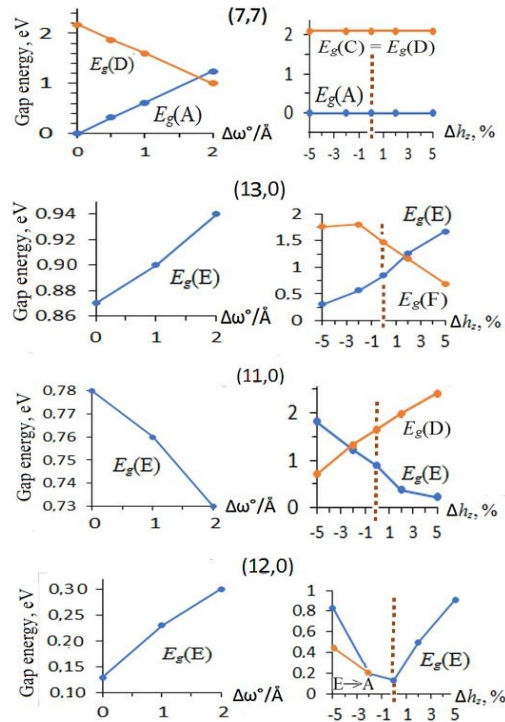


Fig. 5. Band structure changes under twisting the (7,7) SWNT.

The torsion opens the  $E_g(A)$  gap, and it quickly increases up to the 1.3 eV at the  $\Delta\omega$  angle of  $2^\circ/\text{\AA}$ . The direct gaps at the C, E, and G points become larger, and the gaps at the points D, F, and H decrease due to such deformations of this material. At  $\Delta\omega = 2^\circ/\text{\AA}$ , the gap  $E_g = 1.0$  eV at the D point with  $L = 6$  turns out to be  $\sim 0.3$  eV smaller as compared to the  $E_g(A)$  gap. Initially, the minimum gap quickly grows from zero to about 1.1 eV, next jumps from points A to D of the Brillouin zone, and finally decreases. Coinciding with the TB approach [22,24,36], in the armchair SWNT, a metal-semiconductor transition independent of the twisting direction is observed, which effectively controls the carbon nanotube spring conductivity.

In contrast to twisting, the uniaxial tensions of armchair SWNT do not open any gap at point A. Moreover, at all other points B, ..., H, the electronic levels' shifts due to the stretching and compression of the tubule are visually almost indistinguishable in the band diagrams and quantitatively insignificant. Thus, the band structure of the armchair SWNT is changed drastically under the twisting, but it is virtually retained under the uniaxial deformations of the tubule (Fig. 6).



**Fig. 6.** Minimum band gap changes under twisting  $\Delta\omega$  and uniaxial tension  $\Delta h_z$  of nonchiral SWNTs.

### 3.3. Zigzag SWNTs

The band structure of the (13,0)  $p = 1$  nanotube is presented in Fig. 7. For the ideal untwisted tubule, the minimum gap  $E_g(E) = 0.85$  eV ( $L = 9$ ) and the energy of the second direct gap  $E_g(F)$  is equal to about 1.5 eV ( $L = 8$ ). All other gaps are above 2.5 eV. Twisting the tube at  $\Delta\omega \leq 2^\circ/\text{\AA}$  results in a weak change of the electronic structure only. Thus, the minimum gap  $E_g(E)$  increases to 0.94 eV only, and changes in the energies of other direct transitions are limited to 0.1 eV. The positive sign of minimum band gap derivative  $dE_g(E)/d\Delta\omega$  is the same as predicted in the Hückel model for the SWNTs of this family [22,23]. On the contrary, Fig. 6 shows that uniaxial deformations of this tubule strongly disturb the electronic energy levels, changing even the boundary band order. Stretching the tube within 5% leads to a rapid increase (twofold at  $\Delta h_z = 5\%$ ) in the gap at point E and the same decrease in the transition energy at point F. Near the  $\Delta h_z = 2\%$ , the gaps coincide,  $E_g(E) \approx E_g(F) \approx 1.2$  eV, and then an inversion of the order of gaps at these points of the Brillouin zone is observed. The contraction of this tube is accompanied by the drop in the  $E_g(E)$  gap from 0.85 eV to 0.33 eV and an increase in the  $E_g(F)$  value to 1.8 eV. At  $\Delta h_z = 0$ , the sign of the derivative of the width of the minimum forbidden band  $dE_g(E)/dh_z$  is positive, as it is expected for tubes of the family  $p = 1$  [22,23], and the sign of the derivative  $dE_g(F)/dh_z$  is negative.

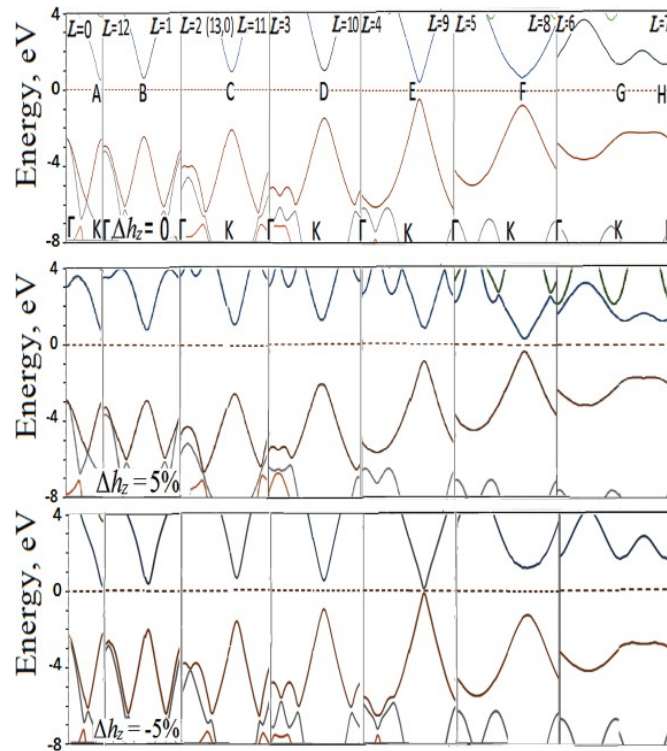


Fig. 7. Variation of band structure of (13,0) SWNT due to stretching ( $\Delta h_z > 0$ ) and compression ( $\Delta h_z < 0$ )

Similar to the (13,0) case, twisting the semiconducting (11,0)  $p = -1$  SWNT is accompanied by a weak change in the electron levels (Fig. 8). In the ideal (11,0) nanotube, the minimum direct gap  $E_g(E) = 0.78$  eV corresponds to electronic transition at the E point and  $L = 7$ . Twisting this tubule up to the  $\Delta\omega \leq 2^\circ/\text{\AA}$  results in a decrease in the gap by 0.05 eV only. The energies of all other direct gaps are equal to the 1.6 eV or larger and their average variations are about 0.1 eV. The extension and compression have a strong effect on the electronic structure of the (11,0) tubule. Here, an intersection of the two minimum gaps  $E_g(E)$  and  $E_g(F)$  is observed under the compression with  $\Delta h_z = -2\%$ . For an approximately threefold decrease in the optical gap, one must stretch the tube (11,0) by 5%. Here, for the main minimum gap,  $dE_g(E)/dh_z < 0$ , and for the second gap,  $dE_g(D)/dh_z > 0$ . Thus, within the considered deformations, the semiconducting zigzag tubules are rigid to mechanical twisting, but not to extension or contraction. For NEMS devices, the tubules with resistant to torsion and sensitive to axial deformations are required.

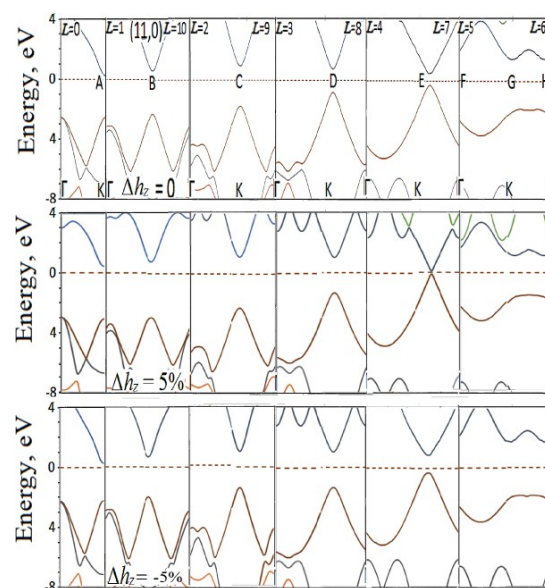


Fig. 8. Variation of band structure of (11,0) SWNT due to stretching and compression.

Figures 6 and 9 show that there is the minigap  $E_g = 0.04$  eV at point E ( $L = 8$ ) in the ideal quasi-metallic  $(12,0)$   $p = 0$  zigzag SWNT. It is the narrow-gap semiconductor due to the effects of the nanotube's surface curvature. In this tube, the band gap  $E_g(E)$  increases any time when it is twisted, stretched, or compressed. An increase in the  $\Delta\omega$  twist angle from zero to  $2^\circ/\text{\AA}$  is accompanied by growth in the minimum gap up to 0.3 eV only. The change is smaller than the variation of the gap in the quasi-metallic chiral  $(9,6)$  SWNT due to twisting. The stretching leads to the faster growth of the gap  $E_g(E)$  up to the 0.91 eV at  $\Delta h_z = 5\%$ . When the tube is compressed by 5%, the energy of the direct transition  $E_g(E)$  reaches 0.83 eV, but this transition competes with an indirect gap between the states  $E_v(E)$  and  $E_c(A)$  with energy gap equal to 0.45 eV at  $\Delta h_z = -5\%$ .

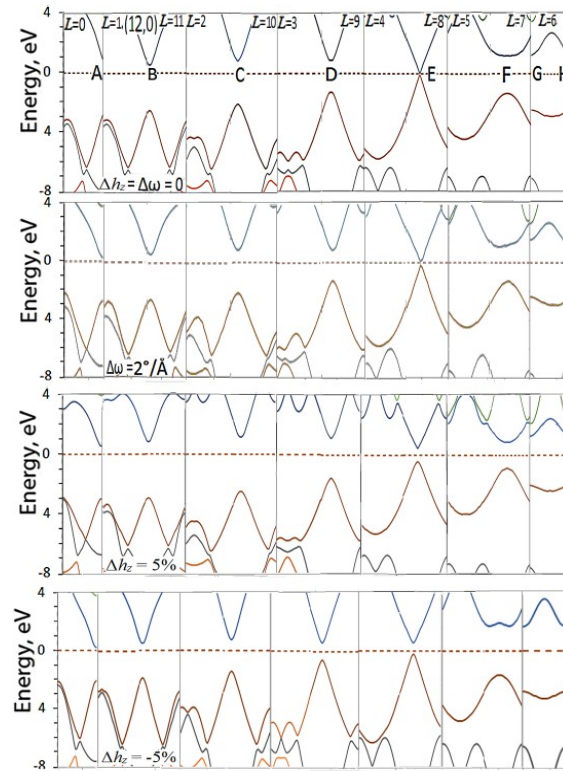


Fig. 9. Band structure change under twisting  $\Delta\omega$ , stretching, and compression  $\pm\Delta h_z$   $(12,0)$  SWNT.

#### 4. Conclusions

The effects of twisting and axial tensions on the band structures of chiral and achiral SWNTs were quantitatively investigated in detail in the framework of the LACW theory. Due to the account of all symmetry operations, the computational costs for all tubules are the same with all twisting, compression, and extension deformations. It is found that even relatively small perturbations of the SWNTs geometry strongly affect not only the minimum band gap but also the energies of other direct and indirect optical transitions. In the chiral semiconducting tubules, the induced shifts of the first and second gaps are opposite, and an inversion of the order of gaps as well as metallization takes place under the twisting and axial modes. In the metallic and quasi-metallic tubules, a transition to the semiconducting states is observed regardless of the direction of even small twisting, but their band structures are rigid to axial deformations. In achiral semiconductor tubes, the band structure, including the order of the boundary bands, changes strongly upon stretching, but the effects of twisting are weaker in an order of magnitude. These results show that the optical and electrical properties of SWNTs can be controlled just by applying suitable deformations.

**Funding:** This research was funded by Russian Science Foundation. Grant No. 22-23-00154, <https://rscf.ru/project/22-23-00154/>.

**Conflicts of Interest:** The author declares no conflict of interest. The funders had no role in the design of the study; in the collection, analyses, or interpretation of data; in the writing of the manuscript, or in the decision to publish the results.

## References

- Iijima, S. Helical microtubules of graphitic carbon. *Nature* **1991**, *354*, 56. <https://doi.org/10.1038/354056a0>
- Mintmire, J. W.; Dunlop, B. I.; White, C. T. Are fullerene tubules metallic? *Phys. Rev. Lett.* **1992**, *68*, 631. <https://doi.org/10.1103/PhysRevLett.68.631>
- Saito, R.; Fujita, M.; Dresselhaus, G.; Dresselhaus, M. S. Electronic structure of chiral graphene tubules. *Appl. Phys. Lett.* **1992**, *60*, 2204. <https://doi.org/10.1063/1.107080>
- Saito, R.; Fujita, M.; Dresselhaus, G.; Dresselhaus, M. S. Electronic structure of graphene tubules based on C60. *Phys. Rev. B* **1992**, *46*, 1804. <https://doi.org/10.1103/PhysRevB.46.1804>
- Hamada, N.; Sawada, S.; Oshiyama, A. New one-dimensional conductors: graphitic microtubules. *Phys. Rev. Lett.* **1992**, *68*, 1579–1581. <https://doi.org/10.1103/PhysRevLett.68.1579>
- Elise, Y. Li.; Marzari, N. A. Natural helical crystal lattice model for carbon nanotubes. *J. Chem. Theory Comput.* **2013**, *9*, 4, 1865–1871. <https://doi.org/10.1021/ct301007h>
- Ghorbani-Asl, M.; Juarez-Mosqueda, R.; Kuc, A.; Heine, T. Efficient quantum simulations of metals within the  $\Gamma$ -point approximation: application to carbon and inorganic 1D and 2D materials. *J. Chem. Theory Comput.* **2012**, *8*, 2888–2895. <https://doi.org/10.1021/ct3003496>
- White, C. T.; Robertson, D. H.; Mintmire, J. W. Helical and rotational symmetries of nanoscale graphitic tubules. *Phys. Rev. B* **1993**, *47*, 5485. <https://doi.org/10.1103/PhysRevB.47.5485>
- Lu, J. P. Elastic properties of carbon nanotubes and nanoropes. *Phys. Rev. Lett.* **1997**, *79*, 1297–1230. <https://doi.org/10.1103/PhysRevLett.79.1297>
- Changa, T. Torsional behavior of chiral single-walled carbon nanotubes is loading direction dependent. *Appl. Phys. Lett.* **2007**, *90*, No. 201910. <https://doi.org/10.1063/1.2739325>
- Minot, E. D.; Yaish, Y.; Sazonova, V.; Park, J.-Y.; Brink, M.; McEuen, P. L. Tuning carbon nanotube band gaps with strain. *Phys. Rev. Lett.* **2003**, *90*, No. 156401. <https://doi.org/10.1103/PhysRevLett.90.156401>
- Sazonova, V.; Yaish, Y.; Üstünel, H.; Roundy, D.; Arias, T.A.; McEuen, P.L. A Tunable carbon nanotube electromechanical oscillator. *Nature* **2004**, *431* 6 284–287. <https://doi.org/10.1038/nature02905>
- Tombler, T. W.; Zhou, C.; Alexseyev, L.; Kong, J.; Dai, H.; Liu, L.; Jayanthi, C. S.; Tang, M.; Wu, S.-Y. Reversible electromechanical characteristics of carbon nanotubes under local-probe manipulation. *Nature* **2000**, *405*, 769–772. <https://doi.org/10.1038/35015519>
- Gómez-Navarro, C.; de Pablo, P. J.; Gómez-Herrero, J. Radial electromechanical properties of carbon nanotubes. *Adv. Mater.* **2004**, *16*, 549–552. <https://doi.org/10.1002/adma.200305678>
- Semet, V.; Binh, V. T.; Guillot, D. K.; Teo, B. K.; Chhowalla, M.; Amaratunga, G. A. J.; Milne, W. I.; Legagneux, P.; Pribat, D. Reversible electromechanical characteristics of individual multiwall carbon nanotubes. *Appl. Phys. Lett.* **2005**, *87*, No. 223103. <https://doi.org/10.1063/1.2136229>
- Cohen-Karni, T.; Segev, L.; Srur-Lavi, O.; Cohen, S. R.; Joselevich, E. Torsional electromechanical quantum oscillations in carbon nanotubes. *Nature Nanotechnol.* **2006**, *1*, 36–41. <https://doi.org/10.1038/nnano.2007.179>
- Craighead, H. G. Nanoelectromechanical systems. *Science* **2000**, *290*, 1532–1535. <https://doi.org/10.1126/science.290.5496.1532>
- Wang, M. Z. Carbon Nanotube NEMS. In *Encyclopedia of Nanotechnology*. B. Bhushan (ed.). Springer, Dordrecht, 2015; 11 p.
- Chiu, H.Y.; Hung, P.; Postma, H.W.C.; Bockrath, M. Atomic-scale mass sensing using carbon nanotube resonators. *Nano Lett.* **2008**, *8*, 4342–4346. <https://doi.org/10.1021/nl802181c>
- Chaste, J.; Eichler, A.; Moser, J.; Ceballos, G.; Rurali, R.; Bachtold, A. A Nanomechanical mass sensor with yoctogram resolution. *Nature Nanotechnol.* **2012**, *7*, 301–304. <https://doi.org/10.1038/nnano.2012.42>
- Moser, J.; Güttinger, J.; Eichler, A.; Esplandiú, M.J.; Liu, D.E.; Dykman, M.I.; Bachtold, A. Ultrasensitive force detection with a nanotube mechanical resonator. *Nature Nanotechnol.* **2013**, *8*, 493–496. <https://doi.org/10.1038/ncomms3843>
- Jensen, K.; Weldon, J.; Garcia, H.; Zettl, A. Nanotube radio. *Nano Lett.* **2007**, *7*, 11, 3508–3511. <https://doi.org/10.1021/nl0721113>
- Yang, L.; Anantram, M. P.; Han, J.; Lu, J. P. Band-gap change of carbon nanotubes: effect of small uniaxial and torsional strain. *Phys. Rev. B* **1999**, *60*, 13874–13878. <https://doi.org/10.1103/PhysRevB.60.13874>
- Yang L.; Han, J. Electronic Structure of Deformed Carbon Nanotubes. *Phys. Rev. Lett.* **2000**, *85*, 154–157. <https://doi.org/10.1103/PhysRevLett.85>
- Kane, C. L.; Mele, E. J. Size, shape, and low energy electronic structure of carbon nanotubes. *Phys. Rev. Lett.* **1997**, *78*, 10, 1932–1935. <https://doi.org/10.1103/PhysRevLett.78.1932>
- Bundera, J. E.; Hill, J. M. Electronic properties of carbon nanotubes with distinct bond lengths. *J. Appl. Phys.* **2010**, *107*, No. 023511. <https://doi.org/10.1063/1.3289320>
- Heyd, R.; Charlier, A.; McRae, E. Uniaxial-stress effects on the electronic properties of carbon nanotubes. *Phys. Rev. B* **1997**, *55*, 6820–6824. <https://doi.org/10.1103/PhysRevB.55.6820>

28. Dmitrović, S.; Milošević, I.; Damnjanović, M.; Vuković, T. Electronic properties of strained carbon nanotubes: impact of induced deformations. *J. Phys. Chem. C* **2015**, *119*, 24, 13922–13928. <https://doi.org/10.1021/acs.jpcc.9b10718>
29. Rochefort, A.; Avouris, P.; Lesage, F.; Salahub, D. R. Electrical and mechanical properties of distorted carbon nanotubes. *Phys. Rev. B* **1999**, *60*, 13824–13830. <https://doi.org/10.1103/PhysRevB.60.13824>
30. Bailey, S. W. D.; Tomanek, D.; Kwon, Y.-K.; Lambert, C. J. Giant magneto-conductance in twisted carbon nanotubes. *Europhys. Lett.* **2002**, *59*, 1, 75–80. <https://doi.org/10.1209/epl/i2002-00161-8>
31. Maiti, A. Mechanical deformation in carbon nanotubes – bent tubes vs tubes pushed by atomically sharp tips. *Chem. Phys. Lett.* **2000**, *331*, 21–25. [https://doi.org/10.1016/S0009-2614\(00\)01138-6](https://doi.org/10.1016/S0009-2614(00)01138-6)
32. Juarez-Mosqueda, R.; Ghorbani-Asl, M.; Kuc, A.; Heine, T. Electromechanical properties of carbon nanotubes. *J. Phys. Chem. C* **2014**, *118*, 25, 13936–13944. <https://doi.org/10.1021/jp502267d>
33. Ivanovskaya, V. V.; Ranjan, N.; Heine, T.; Merino, G.; Seifert, G. Molecular dynamics study of the mechanical and electronic properties of carbon nanotubes. *Small* **2005**, *1*, 399–402. <https://doi.org/10.1002/sml.200400110>
34. Mazzoni, M. S. C.; Chacham, H. Atomic restructuring and localized electron states in a bent carbon nanotube: a first-principles study. *Phys. Rev. B* **2000**, *61*, 7312–7315. <https://doi.org/10.1103/PhysRevB.61.7312>
35. Gülseren, O.; Yildirim, T.; Ciraci, S.; Kılıç, Ç. Reversible band-gap engineering in carbon nanotubes by radial deformation. *Phys. Rev. B* **2002**, *65*, No. 155410. <https://doi.org/10.1103/PhysRevB.65.155410>
36. Zhang, D.-B.; James, R. D.; Dumitrică, T. Electromechanical characterization of carbon nanotubes in torsion via symmetry adapted tight-binding objective molecular dynamics. *Phys. Rev. B* **2009**, *80*, No. 155418. <https://doi.org/10.1103/PhysRevB.80.115418>
37. Xue, B.; Shao, X.; Cai, W. Comparison of the properties of bent and straight single-walled carbon nanotube intramolecular junctions. *J. Chem. Theory Comput.* **2009**, *5*, 6, 1554–1559. <https://doi.org/10.1021/ct900039v>
38. Kato, K.; Koretsune, T.; Saito, S. Twisting effects on carbon nanotubes: a first-principles study with helical symmetry operations. *J. Phys.: Conf. Ser.* **2011**, *302*, No. 012007. <https://doi.org/10.1088/1742-6596/302/1/012007>
39. Kato, K.; Koretsune, T.; Saito, S. Energetics and electronic properties of twisted single-walled carbon nanotubes. *Phys. Rev. B* **2012**, *85*, No. 115448. <https://doi.org/10.1103/PhysRevB.85.115448>
40. Liu, L.; Jayanthi, C. S.; Tang, M.; Wu, S. Y.; Tomblor, T. W.; Zhou, C.; Alexseyev, L.; Kong, J.; Dai, H. Controllable reversibility of and sp<sup>2</sup> to sp<sup>3</sup> transition of a single-wall nanotube under the manipulation of an AFM tip: a nanoscale electromechanical switch? *Phys. Rev. Lett.* **2000**, *84*, 4950–4953. <https://doi.org/10.1103/PhysRevLett.84.4950>
41. Liu, L.; Jayanthi, C. S.; Wu, S. Y. Structural and electronic properties of a carbon nanotorus: effects of delocalized and localized deformations. *Phys. Rev. B* **2001**, *64*, No. 33412. <https://doi.org/10.1103/PhysRevB.64.033412>
42. Nardelli, M. B.; Fattebert, J.-L.; Orlikowski, D.; Roland, C.; Zhao, Q.; Bernholc, J. Mechanical properties, defects and electronic behavior of carbon nanotubes. *Carbon* **2000**, *38*, 1703–1711. [https://doi.org/10.1016/S0008-6223\(99\)00291-2](https://doi.org/10.1016/S0008-6223(99)00291-2)
43. Nardelli, M. B. Electronic transport in extended systems: application to carbon nanotubes. *Phys. Rev. B* **1999**, *60*, 7828–7833. <https://doi.org/10.1103/PhysRevB.60.7828>
44. Nardelli, M. B.; Bernholc, J. Mechanical deformations and coherent transport in carbon nanotubes. *Phys. Rev. B* **1999**, *60*, R16338–R16341.
45. Joselevich, E. Twisting nanotubes: from torsion to chirality. *ChemPhysChem* **2006**, *7*, 1405–1407. <https://doi.org/10.1002/cphc.200600206>
46. D'yachkov, P. N.; Makaev, D. V. Account of helical and rotational symmetries in the linear augmented cylindrical wave method for calculating the electronic structure of nanotubes: towards the ab initio determination of the band structure of a (100, 99) tubule. *Phys. Rev. B* **2007**, *76*, No. 195411. <https://doi.org/10.1103/PhysRevB.76.195411>
47. D'yachkov, P. N. Linear augmented cylindrical wave method for nanotubes electronic structure. *Intern. J. Quantum Chem.* **2016**, *116*, 174–188. <https://doi.org/10.1002/qua.25000>
48. D'yachkov, P. N.; Makaev, D. V. Ab initio spin-dependent band structures of carbon nanotubes. *Intern. J. Quantum Chem.* **2016**, *116*, 316–324. <https://doi.org/10.1002/qua.25030>
49. D'yachkov, P. N. Quantum chemistry of nanotubes: electronic cylindrical waves. CRC Press. Taylor and Francis. London and New York, 2019; 212 p.
50. D'yachkov, E. P.; D'yachkov, P. N. Gold nanosolenoids based on chiral nanotubes calculated using the relativistic linearized augmented cylindrical wave method. *J. Phys. Chem. C* **2019**, *123*, 42, 26005–26010. <https://doi.org/10.1021/acs.jpcc.9b07610>
51. Slater, J. C. Wave functions in a periodic potential. *Phys. Rev.* **1937**, *51*, 851. <https://doi.org/10.1103/PhysRev.51.846>
52. Slater, J. C. The self-consistent field for molecules and solids, quantum chemistry of molecules and crystals, Vol. 4; McGraw-Hill: New York, 1974.
53. Andersen, O. K. Linear methods in band theory. *Phys. Rev. B* **1975**, *12*, 3060–3083. <https://doi.org/10.1103/PhysRevB.12.3060>
54. Koelling, D. D.; Arbman, G. O. Use of energy derivative of the radial solution in an augmented plane wave method: application to copper. *J. Phys. F: Met. Phys.* **1975**, *5*, 2041–2054. <https://doi.org/10.1088/0305-4608/5/11/016>

**Publisher's Note:** IIKII stays neutral with regard to jurisdictional claims in published maps and institutional affiliations.

**Copyright:** © 2022 The Author. Published with license by IIKII, Singapore. This is an Open Access article distributed under the terms of the [Creative Commons Attribution License](#) (CC BY), which permits unrestricted use, distribution, and reproduction in any medium, provided the original author and source are credited.